

We are grateful to the referee for providing helpful comments and guidance that have improved the manuscript. In this document, we describe how we have addressed the reviewer's comments. Referee comments are shown in black italics and author responses are shown in blue regular text. A manuscript with tracking changes is attached at the end.

Thanks to the authors for taking into consideration my previous comments. In this round, I only have one more question and a few suggestions to the language.

The authors used a dynamic vegetation model to examine impacts of differing scenarios on ecosystem carbon sequestration across China, which, however, is decoupled from the regional climate. I am curious if ecosystem-climate interactions were accounted for, how would the allowable carbon budget change (if any)?

→ We could not answer the possible impacts of ecosystem-climate interactions on allowable carbon budget as raised by the reviewer, because this requires a totally different research tool. In this study, ecosystem carbon assimilation responds to climate change without feedback. The full coupling among ecosystems, atmospheric chemistry, and climate has been examined in our previous studies (Yue et al., 2017a; Yue et al., 2017b). For those studies, climate was simulated using a single model NASA ModelE2-YIBs. However, for this study, “we do not consider ecosystem-climate interactions as in the earlier studies (e.g., Yue et al., 2017), so as to take advantage of climate projections from multiple models.” (Lines 252-254)

A few more suggestions to the text:

L44: change ‘pollution’ to ‘pollutants’

→ Corrected as suggested.

L67-71: references could be added.

→ A related study introducing both transient and stabilized pathways to 1.5°C was added as follows:

James, R., Washington, R., Schleussner, C. F., Rogelj, J., and Conway, D.: Characterizing half-a-degree difference: a review of methods for identifying regional climate responses to global warming targets, *Wires Clim Change*, 8, e457, 2017.

L74-75: similarly, any refs here to justify 1.5 can be broken under a transient pathway?

→ A related study projected that the 1.5°C warming target could be reached before the year 2029, and might be even earlier by the year 2026 if with positive phase of

Interdecadal Pacific Oscillation. It has been added as follows:

Henley, B. J., and King, A. D.: Trajectories toward the 1.5 degrees C Paris target: Modulation by the Interdecadal Pacific Oscillation, *Geophys Res Lett*, 44, 4256-4262, 2017.

L128: language error: one option is to replace the comma between ‘...present day’ and ‘meanwhile’ with semicolon.

→ Corrected as suggested.

L220: performed.

→ Corrected as suggested.

L205-206: I think a more precise expression should be “meta-analyses of hundreds of data from China and the world’.

→ Corrected as suggested.

L235: change ‘fix’ to ‘fixed’

→ We consider it might be better to use present tense here.

L248: change among to between.

→ Corrected as suggested.

L393: change allow to allows

→ Corrected as suggested.

References

Yue, X., Strada, S., Unger, N., and Wang, A.: Future inhibition of ecosystem productivity by increasing wildfire pollution over boreal North America, *Atmospheric Chemistry and Physics*, 17, 13699-13719, 10.5194/acp-17-13699-2017, 2017a.

Yue, X., Unger, N., Harper, K., Xia, X., Liao, H., Zhu, T., Xiao, J., Feng, Z., and Li, J.: Ozone and haze pollution weakens net primary productivity in China, *Atmospheric Chemistry and Physics*, 17, 6073-6089, 10.5194/acp-17-6073-2017, 2017b.

1 **Pathway dependence of ecosystem responses in China to 1.5°C global warming**

2
3 Xu Yue¹, Hong Liao¹, Huijun Wang², Tianyi Zhang³, Nadine Unger⁴, Stephen Sitch⁴,
4 Zhaozhong Feng¹ and Jia Yang⁵

5
6
7 ¹ Jiangsu Key Laboratory of Atmospheric Environment Monitoring and Pollution Control,
8 Collaborative Innovation Center of Atmospheric Environment and Equipment Technology, School
9 of Environmental Science and Engineering, Nanjing University of Information Science &
10 Technology (NUIST), Nanjing, 210044, China

11 ² Ministry of Education Key Laboratory of Meteorological Disaster, Joint International Research
12 Laboratory of Climate and Environment Change, Collaborative Innovation Center on Forecast and
13 Evaluation of Meteorological Disasters, NUIST, Nanjing, 210044, China

14 ³ State Key Laboratory of Atmospheric Boundary Layer Physics and Atmospheric Chemistry,
15 Institute of Atmospheric Physics, Chinese Academy of Sciences, Beijing, 100029, China

16 ⁴ College of Engineering, Mathematics and Physical Sciences, University of Exeter, Exeter, EX4
17 4QE, UK

18 ⁵ Department of Forestry, Mississippi State University, Mississippi State, MS, 39762, US

19
20 Email: yuexu@nuist.edu.cn and hongliao@nuist.edu.cn

21
22
23
24
25

26
27
28
29
30
31
32
33
34
35
36
37
38
39
40
41
42
43
44
45
46
47
48
49

Abstract

China is currently the world's largest emitter of both CO₂ and short-lived air pollutants. The ecosystems in China help mitigate a part of its carbon emissions, but are subject to perturbations in CO₂, climate, and air pollution. Here, we use a dynamic vegetation model and data from three model inter-comparison projects to examine ecosystem responses in China under different emission pathways towards the 1.5°C warming target set by the Paris Agreement. At 1.5°C warming, gross primary productivity (GPP) increases by 15.5±5.4 % in a stabilized pathway and 11.9±4.4 % in a transient pathway. CO₂ fertilization is the dominant driver of GPP enhancement and climate change is the main source of uncertainties. However, differences in ozone and aerosols explain the GPP differences between pathways at 1.5°C warming. Although the land carbon sink is weakened by 17.4±19.6 % in the stabilized pathway, the ecosystems mitigate 10.6±1.4% of national emissions in the stabilized pathway, more efficient than the fraction of 6.3±0.8% in the transient pathway. To achieve the 1.5°C warming target, our analysis suggests a higher allowable carbon budget for China under a stabilized pathway with reduced emissions in both CO₂ and air pollutants.

Deleted: pollution

Keywords: Ecosystems, climate change, 1.5°C warming, emission pathway, ozone vegetation damage

51 **1 Introduction**

52 The past decade has seen record-breaking warming largely related to anthropogenic
53 greenhouse gas emissions (Mann et al., 2017). This warming trend presents a challenge
54 to achieve the temperature control target of 1.5°C above the pre-industrial (PI) level set
55 by the 2015 Paris climate agreement. Many studies have shown that a conservative
56 warming such as 1.5°C is necessary to limit climatic extremes (Nangombe et al., 2018),
57 avoid heat-related mortality (Mitchell et al., 2018), reduce economic loss (Burke et al.,
58 2018), and alleviate ecosystem risks (Warszawski et al., 2013) compared to stronger
59 anthropogenic warming. To achieve this target, each country must aim to control its
60 greenhouse gas emissions. A full understanding of regional ecosystem response to the
61 changing climate and environmental stress is essential to reduce uncertainties in
62 allowable carbon budget estimates at 1.5°C (Mengis et al., 2018). China is covered with
63 a wide range of terrestrial biomes (Fang et al., 2012). While China's ecosystem
64 response to possible future climate has been explored (Wu et al., 2009; He et al.,
65 2017; Dai et al., 2016), impacts on the regional carbon budget of differing pathways to
66 the 1.5°C target are not known.

67

68 There are two distinct pathways to the 1.5°C global warming. One is a fast process in
69 which global temperature passes 1.5°C and continues to increase (scenarios assuming
70 high CO₂ emissions and no climate mitigation) while the other is a stabilized process
71 with an equilibrium warming right below 1.5°C and last for decades before the end of
72 21st century (scenarios including climate mitigation) (James et al., 2017). The stabilized
73 pathway is the one proposed by the 2015 Paris agreement. However, the unprecedented
74 warming in 2016 results in an increase of global average temperature by 1.1°C above
75 PI (<https://public.wmo.int>), suggesting that the 1.5°C limit can be broken in a near
76 future under a transient pathway, (Henley and King, 2017). A few studies have
77 compared allowable carbon budgets between these two pathways (Collins et al.,
78 2018; Millar et al., 2017), but none has estimated the mitigation potential of regional
79 ecosystems with joint impacts of changes in climate, CO₂, and air pollution under
80 different pathways.

Deleted: .

Deleted: .

83

84 Here, we apply the Yale Interactive terrestrial Biosphere Model (YIBs) (Yue and Unger,
85 2015; Yue and Unger, 2018) to investigate the response of terrestrial ecosystem
86 productivity in China to both stabilized and transient global warming of 1.5°C relative
87 to PI period. We focus on the changes of gross primary productivity (GPP) and net
88 ecosystem exchange (NEE). GPP represents the total canopy photosynthesis through
89 gross carbon assimilation. NEE is the residue after subtraction of GPP from ecosystem
90 (plant plus soil) respiration (Reco – GPP), indicating the net carbon sink from land to
91 atmosphere. The larger the GPP values, the stronger carbon assimilation by ecosystems.
92 In contrast, the more negative the NEE, the stronger carbon sink of land. The YIBs
93 model is driven with meteorology from an ensemble of climate models in Climate
94 Model Intercomparison Project Phase 5 (CMIP5). The stabilized global warming
95 pathway is represented by the RCP2.6 low emissions scenario that yields an equilibrium
96 change in Global Mean Temperature (Δ GMT) of 1.49°C by 2050-2070 with selected
97 climate models (Fig. S1). The transient pathway is represented by RCP8.5 high
98 emission scenario in which Δ GMT grows rapidly and realizes a transient 1.5°C around
99 the year 2021-2041. We select the present-day period of 1995-2015 as a reference.

100

101

102 **2 Methods**

103 **2.1 Datasets**

104 **2.1.1 CMIP5 data**

105 We use both daily and monthly meteorology predicted by CMIP5 models
106 (<https://cmip.llnl.gov/>). The daily data are used as input for YIBs model. In total, we
107 select 15 climate models (Table S1) with all available daily meteorology, including
108 surface air temperature, precipitation, specific humidity, surface downward shortwave
109 radiation, surface pressure, and surface wind speed, for historical and two future
110 scenarios (RCP2.6 and RCP8.5). These two scenarios assume distinct emission
111 pathways of both CO₂ and air pollutants, with the RCP2.6 scenario projecting much
112 lower CO₂ and pollution concentrations than RCP8.5. Simulated annual GMT is

113 smoothed with a 21-year window to remove decadal variations. The ensemble changes
114 of GMT relative to PI period (1861-1900) from two scenarios are examined (Fig. S1a).
115 The low emission scenario RCP2.6 yields an equilibrium Δ GMT of 1.85°C by 2100.
116 We remove 8 climate models predicting stabilized Δ GMT higher than 1.85°C by the
117 end of century. The 7 remaining models yield an ensemble warming close to 1.5°C
118 (1.49°C for 2050-2070, Fig. S1b). Meanwhile, Δ GMT in the high emission scenario
119 RCP8.5 grows fast and realizes a transient 1.5°C warming around the year 2021-2041.
120 Daily meteorology from 7 selected models (Table S1) are then interpolated to the
121 uniform $1^\circ \times 1^\circ$ resolution and used to drive YIBs model to simulate terrestrial carbon
122 fluxes in China for 1850-2100. Due to the large data storage, we retain only the domain
123 of [15-60°N, 60-150°E] covering China territory. We bias correct modeled meteorology
124 with WFDEI (WATCH Forcing Data methodology applied to ERA-Interim reanalysis)
125 data (Weedon et al., 2014):

126

$$127 \quad V_d^s = V_d \times S_w / S_m \quad (1)$$

128

129 Here V_d is the original daily variables and V_d^s is the scaled value. S_w is the 2-
130 dimensional WFDEI value averaged for 1980-2004 and S_m is the modeled values
131 averaged at the same period. In this case, the average climate from each individual
132 model matches observations at present day, meanwhile, climate variability from models
133 are retained to estimate uncertainties in carbon fluxes.

134

135 2.1.2 TRENDY-v6 data

136 We acquire the global GPP and NEE datasets from 1901 to 2016 simulated by 14
137 Dynamic Global Vegetation Models (DGVMs) participating in TRENDY project
138 (Table S2). All DGVMs are implemented following the same simulation protocol and
139 driven by consistent input datasets, including CRU-NCEP climate data, atmospheric
140 CO₂ concentrations, but fixed present-day land use (Le Quere et al., 2018).

141

142 2.1.3 ACCMIP O₃ data

Deleted:

144 We use monthly output of surface O₃ concentrations from 12 models joining the
 145 Atmospheric Chemistry and Climate Model Intercomparison Project (ACCMIP,
 146 Lamarque et al., 2013) (Table S3). The ACCMIP models have a wide range of
 147 horizontal and vertical resolutions, natural emissions, chemistry schemes, and
 148 interaction with radiation and clouds. However, these models apply the same
 149 anthropogenic and biomass burning emissions specified for CMIP5 RCP scenarios (e.g.,
 150 RCP2.6 or RCP8.5), though different models perform simulations at different time
 151 slices. Here, we use surface O₃ and interpolate original output to 1°×1° resolution. We
 152 fill the temporal gaps between two adjacent time slices using a linear fitting approach.
 153 In this way, we derive the monthly O₃ from 1850 to 2100 for each model and their
 154 ensemble average at each grid point.

155

156 **2.1.4 Diffuse radiation data**

157 The original CMIP5 archive does not provide diffuse component of shortwave radiation.
 158 Here, we use empirical relations between total and diffuse radiation from 11 studies to
 159 calculate hourly diffuse radiation (Table S4). The diffuse fraction k_d in all equations
 160 depends on clearness index k_t , which is defined as the ratio between global solar
 161 radiation I_t and extra-terrestrial solar radiation I_0 (Ghosh et al., 2017):

$$162 \quad k_t = I_t/I_0 \quad (2)$$

$$163 \quad I_0 = I_{sc} \left[1 + 0.033 \cos \left(\frac{360N}{365} \right) \right] \cos \varphi \quad (3)$$

164 Here $I_{sc} = 1367 \text{ W m}^{-2}$ is solar constant, N is Julian day of the year, and φ is solar zenith.

165 The empirical equations are evaluated using hourly total and diffuse radiation from
 166 Modern-Era Retrospective Analysis for Research and Applications (MERRA)
 167 (Rienecker et al., 2011) during 2008-2012. For each grid in China, we calculate hourly
 168 diffuse radiation (D_c) using MERRA total radiation and compare it with the standard
 169 output (D_m). Statistical metrics including correlation, normalized mean bias (NMB),
 170 and normalized root mean square error (NRMSE) are used to evaluate the performance
 171 of empirical equations:

$$172 \quad \text{NMB} = (\overline{D_c} - \overline{D_m})/\overline{D_m} \quad (4)$$

173
$$\text{NRMSE} = \sqrt{\frac{\sum (D_c - D_m)^2}{n}} / \overline{D_m} \quad (5)$$

174 Here $\overline{D_c}$ and $\overline{D_m}$ are mean values of calculated and MERRA diffuse radiation,
175 respectively. The evaluation is performed month by month for 2008-2012 and n is the
176 number of daytime samples (grids with total radiation $> 5 \text{ W m}^{-2}$). The value of n varies
177 from month to month with a minimum of 540,000 in December 2010. Evaluation shows
178 the empirical model M01 (Lam and Li, 1996) yields the highest correlation and the
179 lowest NRMSE (Fig. S2). As a result, we use M01 model to derive diffuse radiation
180 from CMIP5 models.

181

182 **2.2 Model**

183 We apply the YIBs model (Yue and Unger, 2015; Yue et al., 2017) to simulate historical
184 and future (1850-2100) ecosystem productivity. The YIBs model dynamically
185 calculates LAI and tree height based on carbon assimilation and allocation. Leaf-level
186 photosynthesis is calculated hourly using the well-established Farquhar et al. (1980)
187 scheme and is upscaled to canopy level by the separation of sunlit and shading leaves
188 (Spitters, 1986). Sunlit leaves can receive both direct and diffuse radiation, while
189 shading leaves receive only the diffuse component (Yue and Unger, 2017). The
190 assimilated carbon is in part used for maintenance and growth respiration, and the rest
191 is allocated among leaf, stem, and root for plant growth (Clark et al., 2011). Soil
192 respiration is calculated as the loss of carbon flows among 12 soil carbon pools
193 (Schaefer et al., 2008). The YIBs model considers 9 plant functional types (PFTs)
194 including evergreen needleleaf forest (ENF), deciduous broadleaf forest (DBF),
195 evergreen broadleaf forest (EBF), shrubland, tundra, C3 grassland, C4 grassland, C3
196 cropland, and C4 cropland. The land cover is prescribed based on satellite retrievals
197 from the Moderate Resolution Imaging Spectroradiometer (MODIS) (Hansen et al.,
198 2003) and the Advanced Very High Resolution Radiometer (AVHRR) (Defries et al.,
199 2000). For this study, we fix the land cover to isolate impacts of CO_2 and climatic
200 changes. Other studies also show only moderate changes in vegetation fraction and
201 composition at a low warming level (Warszawski et al., 2013). The YIBs model can be

202 applied at the site, regional, and global scales. The site-level model has been evaluated
203 with measured carbon fluxes from 145 FLUXNET sites (Yue and Unger, 2015). For
204 this study, all simulations are performed at the $1^{\circ}\times 1^{\circ}$ resolution over China. During the
205 period of 1982-2011, YIBs predicts an average GPP of $7.17 \text{ Pg C yr}^{-1}$ in China (Fig.
206 S3), close to the $7.25 \text{ Pg C yr}^{-1}$ estimated in the benchmark product (Jung et al., 2009).

207
208 YIBs model calculates O_3 damage to plant photosynthesis using a flux-based
209 parameterization (Sitch et al., 2007). The inhibition rate of GPP is dependent on both
210 ambient O_3 concentrations and stomatal conductance. Compared to ~~meta-analyses of~~
211 ~~hundreds of~~ data from China (Table S5) and the world (Yue and Unger, 2018), the
212 scheme shows good performance in estimating GPP responses to O_3 for DBF, EBF, C3
213 and C4 herbs (Fig. S4). The predicted O_3 damaging effects to ENF might be
214 underestimated. The YIBs model separates the effects of diffuse and direct light on
215 plant photosynthesis (Spitters, 1986). Simulated GPP responses to direct and diffuse
216 radiation show good agreement with observations at 24 global flux tower sites from
217 FLUXNET network (Yue and Unger, 2018). In general, diffuse radiation is more
218 efficient to enhance canopy photosynthesis compared to the same level of direct
219 radiation.

220

221 2.3 Simulations

222 We perform two main groups of simulations, one for RCP2.6 and the other for RCP8.5.
223 For each group, 7 sub-groups are designed with varied climatic or CO_2 forcings (Table
224 S6). In each sub-group, separate runs are conducted for the YIBs model driven with
225 climate variables from 7 selected CMIP5 models (Table S1), making a total of 98 runs.
226 A baseline group (HIST_2000) is ~~performed~~ with fixed meteorology and CO_2 after the
227 year 2000. Another four sub-group simulations are performed to quantify O_3 effects on
228 photosynthesis (Table S7). These simulations are driven with both CMIP5 meteorology
229 and monthly O_3 concentrations from an ensemble of 12 ACCMIP models. The runs are
230 distinguished with different O_3 damaging sensitivity (high or low) and scenario
231 projections (RCP2.6 or RCP8.5). Monthly O_3 concentrations are downscaled to hourly

Deleted: hundreds of

Deleted: perform

234 step using the diurnal cycle simulated by a chemistry-climate model NASA ModelE2
235 (Schmidt et al., 2014). The O₃-affected GPP or NEE are calculated as the average of
236 simulations with low and high sensitivities.

237

238 For each run, a 251-year simulation is performed with historical climate for 1850-2000
239 and future climate for 2001-2100. For simulations driven with meteorology from the
240 same climate model, all sensitivity tests apply the same climate forcing during historical
241 period but utilize varied forcings after the year 2000. For example, RCP26_CO2 is
242 identical to RCP26_MET for the period of 1850-2000. However, after the year 2000,
243 the former runs fix climatic conditions at the year 2000 but allow changes in CO₂
244 concentrations year by year for 2001-2100 following the pathway projection, while the
245 latter fix CO₂ level at the year 2000 but continue to use day-to-day meteorology after
246 2000. For all simulations, we initialize vegetation and soil carbon pools in the YIBs
247 model with a 200-year spin up by recycling meteorology at the year of 1850.
248 Contributions of individual factors are calculated as the differences between sensitivity
249 and baseline group (e.g., RCP26_CO2 – HIST_2000 for CO₂ fertilization in RCP2.6
250 scenario).

251

252 The main focus of this study is to quantify how the differences of anthropogenic
253 emissions, including both CO₂ and air pollution which are usually associated, will cause
254 different responses in land carbon budget to the same global warming target. Especially,
255 the role of air pollution on land carbon cycle has always been ignored. The assumptions
256 of land use can be quite uncertain between future pathways (Stehfest et al., 2019), and

Deleted: among

257 these assumptions are not necessarily associated with CO₂ and air pollution emissions.

258 As a result, for this study, we consider fixed land cover in all simulations. We do not
259 consider ecosystem-climate interactions as in the earlier studies (e.g., Yue et al., 2017),
260 so as to take advantage of climate projections from multiple models.

261

262 **3 Results**

263 **3.1 Changes of atmospheric compositions and radiation**

265 The ensemble concentrations of ACCMIP O₃ show good agreement with ground-based
266 observations from 1580 sites in China (Fig. 1). The spatial correlation is $R=0.80$ ($p <$
267 0.01) between observations and the ensemble O₃ concentrations ([O₃]), though the latter
268 is higher by 25% (Figs. 1a-1c). Such overestimation is likely attributed to the high [O₃]
269 at night in the models, because the evaluation of maximum daily 8-hour average
270 (MDA8) [O₃], which mainly occurs in the daytime, shows more reasonable predictions
271 with a lower bias of 10% (Figs. 1d-1f). Since the O₃ vegetation damage in general
272 occurs in the daytime, when both plant photosynthesis and [O₃] are at high levels, the
273 ACCMIP [O₃] is good to be used as input for YIBs model to derive long-term O₃
274 inhibition effects on ecosystem productivity.

275

276 The ensemble radiation from CMIP5 models matches observations at 106 sites in China
277 (Fig. 2). For total shortwave radiation, the model prediction shows high values in the
278 West and low values in the Southeast, consistent with observations for a correlation
279 coefficient of $R = 0.79$ ($p < 0.01$) and a mean bias of 8.9%. The derived diffuse radiation
280 is highest in the Southeast, where the total radiation is lowest. Observed diffuse
281 radiation is available only at 17 sites. Compared to these sites, predictions show
282 reasonable spatial distribution with a correlation of $R = 0.65$ ($p < 0.01$) and a low bias
283 of 7.1%. Both the total radiation and derived diffuse radiation are used as input for YIBs
284 model to estimate GPP responses to joint changes in direct and diffuse radiation caused
285 by aerosol removal.

286

287 Atmospheric compositions and radiation show varied changes in different scenarios.
288 The GMT changes mainly follow those in CO₂ concentrations, which show fast growth
289 in RCP8.5 but slow changes in RCP2.6 (Fig. 3a). The latter assumes a large reduction
290 of carbon emissions globally after the year 2020 (Meinshausen et al., 2011). Global
291 CO₂ levels reduce slightly after the year 2030 in RCP2.6, while GMT continues
292 growing until 2050 due to air-sea interactions (Solomon et al., 2009). As a low emission
293 scenario, RCP2.6 experiences a slow growth in nitrogen oxide (NO_x) emissions and a
294 continuous reduction after the year 2020 (Fig. S5), resulting in a decline of 6.4 ppb

295 (15.2%) in surface O₃ over eastern China by 1.5°C warming at 2060 (Fig. 3b). In
296 contrast, RCP8.5 assumes fast growth of NO_x emissions with delayed controls after the
297 year 2030, leading to surface O₃ enhancements of 6.6 ppb (15.7%) by 1.5°C warming
298 at 2030. The lower emissions in RCP2.6 also result in smaller aerosol optical depth
299 (AOD) than RCP8.5 (Fig. S6), leading to higher surface total radiation (Fig. 3c) while
300 lower diffuse radiation (Fig. 3d) due to reducing light extinction (Yu et al., 2006).

301

302 **3.2 Historical ecosystem productivity in China**

303 The ensemble simulations show an increasing trend in GPP in China of 0.011 Pg C yr⁻¹
304 ² over the historical period, 1901-2016 (Fig. 4a). A stronger trend of 0.022 Pg C yr⁻² is
305 found after 1960. Such change is much faster than the trend of 0.013 Pg C yr⁻² estimated
306 by a benchmark product (Jung et al., 2009) for 1982-2011 but close to a recent estimate
307 of 0.02 Pg C yr⁻² combining machine learning algorithms and eddy flux measurements
308 from 40 sites in China (Yao et al., 2018). Simulated trend is also consistent with the
309 TRENDY ensemble, which predicts trends of 0.013 ± 0.006 Pg C yr⁻² (ensemble ± inter-
310 model uncertainty) for 1901-2016 and 0.022 ± 0.01 Pg C yr⁻² for 1961-2016. The YIBs
311 simulations show variabilities of 0.41±0.23 Pg C yr⁻¹ (6.2±3.9%, blue shading in Fig.
312 4a) due to uncertainties in climate from CMIP5 models, much smaller than the value of
313 1.33±0.16 Pg C yr⁻¹ (19.2±2.6%, red shading in Fig. 4a) caused by structural
314 uncertainties across different vegetation models.

315

316 NEE in China is negative, suggesting a regional land carbon sink (Fig. 4b). This sink is
317 -94.7 Tg C yr⁻¹ with a trend of -1.7 Tg C yr⁻² during 1901-2016. Such change matches
318 TRENDY simulations, which predict a multi-model mean carbon sink of -74.1±30.8
319 Tg C yr⁻¹ (uncertainties due to inter-model variations) and a trend of -1.3±0.7 Tg C yr⁻²
320 ² for the same period. During 1980-1989, the ground-based estimate (Piao et al., 2009)
321 suggests a sink of 177±73 Tg C yr⁻¹ in China, consistent with the sink intensity of
322 149±20 Tg C yr⁻¹ from the YIBs ensemble prediction. For the recent period of 1980-
323 2000, YIBs estimates a strengthened sink of 154±30 Tg C yr⁻¹ in China, weaker than
324 the estimate of 198±114 Tg C yr⁻¹ with the DLEM vegetation model (Tian et al., 2011)

325 but is within the estimates of 137-177 Tg C yr⁻¹ based on both ground and satellite data
326 (Fang et al., 2007). The interannual variability in YIBs simulations is much weaker than
327 the estimates in other studies, because the ensemble approach largely dampen variations
328 among different runs. Similar to GPP, the NEE simulations exhibit smaller variability
329 of 62±50 Tg C yr⁻¹ among different YIBs runs than that of 122±57 Tg C yr⁻¹ among
330 different TRENDY models.

331

332 **3.3 Future changes of carbon fluxes**

333 Projected GPP continues to increase in both RCP2.6 and RCP8.5 scenarios after the
334 year 2016 (Fig. S7a). By the global warming of 1.5°C, GPP increases significantly in
335 China, especially over eastern and northeastern parts (Fig. 5). Compared to the present
336 day, GPP with O₃ effects increases by 1.07 ± 0.38 Pg C yr⁻¹ (15.5 ± 5.4 %) in the RCP2.6
337 scenario (Fig. 5a) and 0.82 ± 0.30 Pg C yr⁻¹ (11.9 ± 5.4%) in RCP8.5 (Fig. 5b). The
338 spatial pattern of the GPP changes is similar in the two pathways (correlation coefficient
339 $R=0.93$), except that ΔGPP in RCP2.6 is higher than in RCP8.5 by 30% with a positive
340 center over eastern China (Fig. 5c). Projected NEE continues to be more negative in the
341 RCP8.5 scenario after the year 2016 (Fig. S7b). Meanwhile, future NEE reaches the
342 minimum value (or the maximum sink strength) around the year 2025 and then reverses
343 to be less negative in the RCP2.6 scenario (Fig. S7b). By the period of 1.5°C global
344 warming, NEE changes in China show opposite tendencies between the two pathways.
345 Compared to the present day, NEE increases by 0.03 ± 0.03 Pg C yr⁻¹ (-17.4±19.6 %) in
346 RCP2.6 (Fig. 5d) but decreases by 0.14 ± 0.04 Pg C yr⁻¹ (94.4±24.9 %) in RCP8.5
347 (Fig. 5e), suggesting that land carbon sink is slightly weakened in the former but
348 strengthened in the latter. Their differences exhibit widespread positive values in China
349 with high centers in the East (Fig. 5f).

350

351 The changes in carbon fluxes follow the variations in atmospheric composition and
352 climate (Fig. 6 and Figs. S8-S11). By the global warming of 1.5°C, a dominant fraction
353 of GPP enhancement in China is attributed to CO₂ fertilization (Fig. 6a). For the RCP2.6
354 scenario, CO₂ alone contributes 0.83 Pg C yr⁻¹ (77%) to ΔGPP , with the highest

355 enhancement of $0.8 \text{ g C m}^{-2} \text{ day}^{-1}$ over the southeast coast (Fig. S8a). For RCP8.5, CO_2
356 fertilization increases GPP by $0.95 \text{ Pg C yr}^{-1}$, even higher than the total ΔGPP of 0.82
357 Pg C yr^{-1} . The larger CO_2 -induced ΔGPP in RCP8.5 is due to the higher CO_2
358 concentrations (454 ppm) than RCP2.6 (442 ppm) at the same 1.5°C warming (Fig. 3a).
359 The 12 ppm differences in CO_2 concentrations lead to a change of $0.12 \text{ Pg C yr}^{-1}$ (1.7%)
360 in GPP. This sensitivity of GPP to CO_2 , $0.14\% \text{ ppm}^{-1}$, falls within the range of 0.05-
361 $0.21\% \text{ ppm}^{-1}$ as predicted by 10 terrestrial models (Piao et al., 2013) and that of 0.01-
362 $0.32\% \text{ ppm}^{-1}$ as observed from multiple free-air CO_2 enrichment (FACE) sites
363 (Ainsworth and Long, 2005). The higher ΔGPP in RCP2.6 instead yields a weakened
364 NEE (more positive) due to the CO_2 effects (Fig. 6b). The stabilization of CO_2
365 concentrations in this scenario (Fig. 3a) results in a stabilized GPP after the year 2040
366 (Fig. S7a). Meanwhile, the 55-year (from 2005 to 2060) carbon accumulation enhances
367 soil carbon storage by $10.5 \pm 1.3 \text{ Pg C}$ and promotes soil respiration to $0.71 \pm 0.19 \text{ Pg C}$
368 yr^{-1} . The stabilized GPP while enhanced soil respiration (NEE = Reco – GPP, Reco
369 includes both soil and plant respiration) together lead to a weakened carbon sink (less
370 negative NEE) by 1.5°C warming period (Fig. 7b). In contrast, soil carbon storage
371 increases only $5.2 \pm 0.5 \text{ Pg C}$ in RCP8.5 due to relatively short time period (from 2005
372 to 2031) for carbon accumulation, leading to lower soil respiration of $0.41 \pm 0.15 \text{ Pg C}$
373 yr^{-1} in the fast warming pathway. The continuous increase of GPP and lower soil
374 respiration jointly strengthen the land carbon sink (more negative NEE) in China by 0.1
375 Pg C yr^{-1} under RCP8.5 scenario (Fig. 6a).

376
377 Ozone (O_3) damages plant photosynthesis and the land carbon sink (Sitch et al.,
378 2007; Yue and Unger, 2018). In the present day, O_3 decreases GPP by $6.7 \pm 2.6\%$
379 (uncertainties ranging from low to high damaging sensitivities) in China (Fig. 7d),
380 because of the direct inhibition of photosynthesis by $6 \pm 2.4\%$ (Fig. 7a) and the
381 consequent reduction of $1.8 \pm 0.8\%$ in leaf area index (LAI, Fig. 7g). For 1.5°C global
382 warming, this weakening effect shows opposite tendencies in the two RCP scenarios,
383 with a reduced GPP loss of $4.7 \pm 2.0\%$ in RCP2.6 (Fig. 7e) but an increased loss of
384 $7.9 \pm 3.0\%$ in RCP8.5 (Fig. 7f). These impacts are predominantly driven by the

385 variations of surface O₃ concentrations in the two scenarios, as predicted O₃ at 1.5°C
386 warming decreases by 15.2% in the low emission pathway but increases by 15.7% in
387 the high emission pathway (Fig. 3b). Consequently, changes in O₃ help increase GPP
388 by 0.1±0.03 Pg C yr⁻¹ in RCP2.6 but decrease GPP by 0.14±0.04 Pg C yr⁻¹ in RCP8.5
389 for the same 1.5°C warming. Following the benefits to GPP, the lower O₃ decreases
390 NEE (strengthens the sink) by 0.06±0.02 Pg C yr⁻¹ in RCP2.6, offsetting more than half
391 of the negative effect (weakens the sink) from CO₂ (Fig. 6b). For RCP8.5, O₃ impacts
392 make limited contributions to ΔNEE.

393

394 Changes in meteorology account for the rest of the perturbations in the carbon fluxes.
395 At the global warming of 1.5°C, temperature in China increases by 0.90°C for RCP2.6
396 and 0.91°C for RCP8.5 (Figs. S12a-S12b) compared to present-day climate. The spatial
397 pattern of these changes is very similar without significant differences (Fig. S12c),
398 leading to almost identical GPP responses (Figs. S8d and S9d). Generally, higher
399 temperature is not beneficial for plant photosynthesis at low latitudes (Piao et al., 2013),
400 where regional summer climate is already warmer than the optimal temperature
401 threshold for leaf photosynthesis (Corlett, 2011). As a result, warming leads to negative
402 changes in GPP over the East. Surface specific humidity exhibits widespread
403 enhancement in eastern China (Figs. S13a-S13b). Air humidity may rise in a warmer
404 climate because the corresponding enhancement of saturation pressure ~~allows~~
405 atmosphere to hold more water vapor. On average, surface specific humidity increases
406 by 0.34 g kg⁻¹ in RCP2.6 and 0.31 g kg⁻¹ in RCP8.5, leading to a promotion of GPP by
407 0.14 Pg C yr⁻¹ in the former and a similar value of 0.12 Pg C yr⁻¹ in the latter (Figs. S8e
408 and S9e). Precipitation increases by 0.14 mm day⁻¹ (4.6%) over eastern China in
409 RCP2.6 but decreases by 0.03 mm day⁻¹ (1.2%) in RCP8.5 (Figs. S12d-S12e), leading
410 to higher soil moisture in eastern China for RCP2.6 (Figs. S13d-S13e). Nevertheless,
411 most of vegetation in eastern China is not water stressed, leaving moderate GPP
412 responses to soil moisture changes in both RCP scenarios (Figs. S8f and S9f).

413

414 For the RCP2.6 scenario, the net effect of climate change causes an increase of 0.15 Pg

Deleted: allow

416 C yr⁻¹ in GPP with a range from -0.54 to 0.62 Pg C yr⁻¹ (Fig. 6a). Such large variability
417 in ΔGPP is related to the uncertainties in meteorology from different climate models.
418 For RCP8.5, climate-induced GPP change is only 0.04 Pg C yr⁻¹ with a range from -0.6
419 to 0.26 Pg C yr⁻¹. The discrepancy of ΔGPP for the two pathways is mainly caused by
420 the different radiation impacts, which enhance GPP by 0.2 Pg C yr⁻¹ in RCP2.6 but only
421 0.11 Pg C yr⁻¹ in RCP8.5 (Fig. 6a). Photosynthetically active radiation (PAR) is higher
422 by 2.8 W m⁻² in RCP2.6 than in RCP8.5 (Fig. 3c). The distinct changes in radiation are
423 related to aerosol radiative effects, because global analyses also show radiation
424 enhancement in regions (e.g., U.S. and Europe) with aerosol removal (Fig. S14). The
425 lower AOD in RCP2.6 helps increase solar insolation at surface by reducing light
426 extinction (Yu et al., 2006), and promote precipitation with weaker aerosol semi-direct
427 and indirect effects (Lohmann and Feichter, 2005). Although lower aerosols in RCP2.6
428 slightly decrease diffuse radiation (Fig. 3d), which is more efficient in increasing
429 photosynthesis (Mercado et al., 2009; Yue and Unger, 2018), the overall enhancement
430 in total radiation helps boost GPP. Climate-induced ΔNEE is -0.02 Pg C yr⁻¹
431 (strengthened sink) for both pathways (Fig. 6b), resulting from comparable responses
432 of NEE to changes in radiation ($R=0.82$), temperature ($R=0.71$), air humidity ($R=0.91$),
433 and soil moisture ($R=0.73$) between the two pathways (Figs. S10 and S11).

434

435 **3.4 Impacts on allowable carbon budget**

436 For a warming target of 1.5°C, our analyses suggest that a simultaneous reduction of
437 CO₂ and air pollution emissions enhances the efficiency of land carbon uptake
438 compared to a pathway without air pollution emission control. The increased light
439 availability from aerosol removal and decreased surface O₃ jointly promote GPP in
440 China by 0.3 Pg C yr⁻¹, equivalent to 36% of the CO₂ fertilization. In contrast, air
441 pollution results in a net GPP inhibition of 0.03 Pg C yr⁻¹ under the high emission
442 pathway, suggesting a detrimental environment for plant health. Compared to RCP8.5,
443 the timing of 1.5°C warming is delayed by 30 years in RCP2.6, leading to weaker
444 carbon sink in the latter. However, even with the longer period of accumulation, the
445 total carbon loss by O₃ damage is smaller by 3-16% in RCP2.6 relative to RCP8.5 at

446 the same warming level (Fig. 8a).

447

448 The slow warming increases the allowable cumulative anthropogenic carbon emissions.
449 Assuming China's carbon emission fraction of 27% of the world (the level at year 2017)
450 (Le Quere et al., 2018), the total national emissions allowed are 80.4 Pg C in RCP2.6
451 and 71.9 Pg C in RCP8.5 from the year 2010 to the 1.5°C warming, following the global
452 emission rates defined for these scenarios. The ensemble simulations show that
453 ecosystems in China help mitigate 8.5 ± 1.1 Pg C in RCP2.6 and 4.5 ± 0.6 Pg C in RCP8.5
454 (Fig. 8b). Sensitivity experiments with either reduced CO₂ (but retain high pollution)
455 or reduced pollution (but retain high CO₂) reveal land carbon uptakes of 7.3 ± 0.9 Pg C
456 and 5.0 ± 0.6 Pg C, respectively. These values are both lower than that in RCP2.6,
457 suggesting that simultaneous control of carbon and air pollution emissions can
458 maximize the mitigation potential of ecosystems. The higher ecosystem assimilation
459 rate in a low emission pathway ($10.6 \pm 1.4\%$ in RCP2.6 vs. $6.3 \pm 0.8\%$ in RCP8.5) over
460 China, which is not considered in CMIP5 models, further buffers the pace to the global
461 warming of 1.5°C.

462

463 **4 Discussion and conclusions**

464 Projection of future ecosystem productivity is subject to uncertainties in climate forcing
465 and biophysical responses. The multi-model ensemble is a good approach to reduce the
466 uncertainty in climate (Flato et al., 2013). In this study, we employ daily meteorology
467 from 7 CMIP5 models. A comparison with more CMIP5 models is performed (not
468 shown) and confirms that the changes in meteorology from the 7 selected climate
469 models are robust and representative of future projections. As for ecosystem responses,
470 future projections generally showed increasing GPP in China (Mu et al., 2008; Ji et al.,
471 2008; Ju et al., 2007), however, climate change alone usually reduces productivity by
472 inducing hot and drought weather conditions. In contrast, the YIBs simulations reveal
473 a net positive effect of climate change on GPP though with large uncertainties (Fig. 6a).
474 Such discrepancies are related to structural uncertainties across different vegetation
475 models. Evaluations suggest that biophysical responses to environmental forcings in

476 the YIBs model are generally reasonable as compared to the TRENDY ensemble (Fig.
477 4).

478

479 The YIBs simulations do not consider nitrogen cycle and its limitation on carbon uptake.
480 Inter-model comparisons show that models without nutrient constraints tend to
481 overestimate GPP responses to CO₂ fertilization (Smith et al., 2016). As a result, the
482 difference of CO₂ contributions in RCP scenarios would be smaller than predicted (Fig.
483 6a), suggesting that GPP enhancement in RCP2.6 might be even higher than RCP8.5 if
484 nitrogen cycle is included. In contrast, nitrogen deposition in RCP2.6 would be much
485 smaller than that in RCP8.5 due to emission control (Fig. S5), leading to lower nitrogen
486 supply for ecosystem in the former scenario. Consequently, plant photosynthesis is
487 confronted with stronger nutrient limit in RCP2.6 than that in RCP8.5, resulting in
488 lower CO₂ fertilization efficiency in the former scenario. The net effect of nitrogen
489 cycle on land carbon cycle is very uncertain (Zaehle et al., 2014;Huntzinger et al.,
490 2017;Xiao et al., 2015).

491

492 For a warming target of 1.5°C, our analyses suggest that an associated reduction of CO₂
493 and pollution emissions brings more benefits to ecosystems in China than a pathway
494 without emission control. The slow changes of temperature and other environmental
495 variables due to slow growth of CO₂ are helpful for plant adaptation and limit biome
496 shift (Warszawski et al., 2013), and the lower O₃ and higher solar radiation from aerosol
497 removal increase plant photosynthesis. Consequently, China's ecosystems mitigate
498 10.6±1.4% of national emissions in the stabilized pathway, more efficient than the
499 fraction of 6.3±0.8% in the transient pathway, leaving more allowable carbon budget
500 for economic development and upgrade.

501

502 References

- 503 Ainsworth, E. A., and Long, S. P.: What have we learned from 15 years of free-air CO₂ enrichment
504 (FACE)? A meta-analytic review of the responses of photosynthesis, canopy, *New Phytol*, 165,
505 351-371, [doi:10.1111/J.1469-8137.2004.01224.X](https://doi.org/10.1111/J.1469-8137.2004.01224.X), 2005.
- 506 Burke, M., Davis, W. M., and Diffenbaugh, N. S.: Large potential reduction in economic damages
507 under UN mitigation targets, *Nature*, 557, 549-553, [doi:10.1038/s41586-018-0071-9](https://doi.org/10.1038/s41586-018-0071-9), 2018.
- 508 Clark, D. B., Mercado, L. M., Sitch, S., Jones, C. D., Gedney, N., Best, M. J., Pryor, M., Rooney,
509 G. G., Essery, R. L. H., Blyth, E., Boucher, O., Harding, R. J., Huntingford, C., and Cox, P. M.:
510 The Joint UK Land Environment Simulator (JULES), model description - Part 2: Carbon fluxes
511 and vegetation dynamics, *Geosci Model Dev*, 4, 701-722, [doi:10.5194/Gmd-4-701-2011](https://doi.org/10.5194/Gmd-4-701-2011), 2011.
- 512 Collins, W. J., Webber, C. P., Cox, P. M., Huntingford, C., Lowe, J., Sitch, S., Chadburn, S. E.,
513 Comyn-Platt, E., Harper, A. B., Hayman, G., and Powell, T.: Increased importance of methane
514 reduction for a 1.5 degree target, *Environ Res Lett*, 13, 054003, [doi:10.1088/1748-9326/aab89c](https://doi.org/10.1088/1748-9326/aab89c),
515 2018.
- 516 Corlett, R. T.: Impacts of warming on tropical lowland rainforests, *Trends Ecol Evol*, 26, 606-613,
517 [doi:10.1016/j.tree.2011.06.015](https://doi.org/10.1016/j.tree.2011.06.015), 2011.
- 518 Dai, E. F., Wu, Z., Ge, Q. S., Xi, W. M., and Wang, X. F.: Predicting the responses of forest
519 distribution and aboveground biomass to climate change under RCP scenarios in southern
520 China, *Global Change Biol*, 22, 3642-3661, [doi:10.1111/gcb.13307](https://doi.org/10.1111/gcb.13307), 2016.
- 521 Defries, R. S., Hansen, M. C., Townshend, J. R. G., Janetos, A. C., and Loveland, T. R.: A new
522 global 1-km dataset of percentage tree cover derived from remote sensing, *Global Change Biol*,
523 6, 247-254, [doi:10.1046/J.1365-2486.2000.00296.X](https://doi.org/10.1046/J.1365-2486.2000.00296.X), 2000.
- 524 Fang, J. Y., Guo, Z. D., Piao, S. L., and Chen, A. P.: Terrestrial vegetation carbon sinks in China,
525 1981-2000, *Sci China Ser D*, 50, 1341-1350, [doi:10.1007/s11430-007-0049-1](https://doi.org/10.1007/s11430-007-0049-1), 2007.
- 526 Fang, J. Y., Shen, Z. H., Tang, Z. Y., Wang, X. P., Wang, Z. H., Feng, J. M., Liu, Y. N., Qiao, X. J.,
527 Wu, X. P., and Zheng, C. Y.: Forest community survey and the structural characteristics of
528 forests in China, *Ecography*, 35, 1059-1071, [doi:10.1111/j.1600-0587.2013.00161.x](https://doi.org/10.1111/j.1600-0587.2013.00161.x), 2012.
- 529 Farquhar, G. D., Caemmerer, S. V., and Berry, J. A.: A Biochemical-Model of Photosynthetic Co₂
530 Assimilation in Leaves of C-3 Species, *Planta*, 149, 78-90, [doi:10.1007/Bf00386231](https://doi.org/10.1007/Bf00386231), 1980.
- 531 Flato, G., Marotzke, J., Abiodun, B., Braconnot, P., Chou, S. C., Collins, W., Cox, P., Driouech, F.,
532 Emori, S., Eyring, V., Forest, C., Gleckler, P., Guilyardi, E., Jakob, C., Kattsov, V., Reason, C.,
533 and Rummukainen, M.: Evaluation of Climate Models, in: *Climate Change 2013: The Physical
534 Science Basis. Contribution of Working Group I to the Fifth Assessment Report of the
535 Intergovernmental Panel on Climate Change*, edited by: Stocker, T. F., Qin, D., Plattner, G. K.,
536 Tignor, M., Allen, S. K., Boschung, J., Nauels, A., Xia, Y., Bex, V., and Midgley, P. M.,
537 Cambridge University Press, Cambridge, United Kingdom and New York, NY, USA, 2013.
- 538 Ghosh, A., Norton, B., and Duffy, A.: Effect of sky clearness index on transmission of evacuated
539 (vacuum) glazing, *Renewable Energy*, 105, 160-166, [doi:10.1016/j.renene.2016.12.056](https://doi.org/10.1016/j.renene.2016.12.056), 2017.
- 540 Hansen, M. C., DeFries, R. S., Townshend, J. R. G., Carroll, M., Dimiceli, C., and Sohlberg, R. A.:
541 Global Percent Tree Cover at a Spatial Resolution of 500 Meters: First Results of the MODIS
542 Vegetation Continuous Fields Algorithm, *Earth Interact*, 7, 1-15, [doi:10.1175/1087-3562\(2003\)007<0001:GPTCAA>2.0.CO;2](https://doi.org/10.1175/1087-3562(2003)007<0001:GPTCAA>2.0.CO;2), 2003.
- 544 He, N. P., Wen, D., Zhu, J. X., Tang, X. L., Xu, L., Zhang, L., Hu, H. F., Huang, M., and Yu, G. R.:
545 Vegetation carbon sequestration in Chinese forests from 2010 to 2050, *Global Change Biol*,

Formatted: Indent: Left: 0 cm, Hanging: 2.02 ch, First line:
-2.02 ch

546 23, 1575-1584, [doi:10.1111/gcb.13479](https://doi.org/10.1111/gcb.13479), 2017.

547 [Henley, B. J. and King, A. D.: Trajectories toward the 1.5 degrees C Paris target: Modulation by](#)

548 [the Interdecadal Pacific Oscillation, *Geophys Res Lett*, 44, 4256-4262,](#)

549 [doi:10.1002/2017gl073480, 2017.](#)

550 Huntzinger, D. N., Michalak, A. M., Schwalm, C., Ciais, P., King, A. W., Fang, Y., Schaefer, K.,

551 Wei, Y., Cook, R. B., Fisher, J. B., Hayes, D., Huang, M., Ito, A., Jain, A. K., Lei, H., Lu, C.,

552 Maignan, F., Mao, J., Parazoo, N., Peng, S., Poulter, B., Ricciuto, D., Shi, X., Tian, H., Wang,

553 W., Zeng, N., and Zhao, F.: Uncertainty in the response of terrestrial carbon sink to

554 environmental drivers undermines carbon-climate feedback predictions, *Scientific Reports*, 7,

555 4765, [doi:10.1038/s41598-017-03818-2](https://doi.org/10.1038/s41598-017-03818-2), 2017.

556 [James, R., Washington, R., Schleussner, C. F., Rogelj, J., and Conway, D.: Characterizing half-a-](#)

557 [degree difference: a review of methods for identifying regional climate responses to global](#)

558 [warming targets, *Wires Clim Change*, 8, e457, doi:10.1002/wcc.457, 2017.](#)

559 Ji, J. J., Huang, M., and Li, K. R.: Prediction of carbon exchanges between China terrestrial

560 ecosystem and atmosphere in 21st century, *Sci China Ser D*, 51, 885-898, [doi:10.1007/s11430-](https://doi.org/10.1007/s11430-008-0039-y)

561 [008-0039-y](https://doi.org/10.1007/s11430-008-0039-y), 2008.

562 Ju, W. M., Chen, J. M., Harvey, D., and Wang, S.: Future carbon balance of China's forests under

563 climate change and increasing CO₂, *J Environ Manage*, 85, 538-562,

564 [doi:10.1016/j.jenvman.2006.04.028](https://doi.org/10.1016/j.jenvman.2006.04.028), 2007.

565 Jung, M., Reichstein, M., and Bondeau, A.: Towards global empirical upscaling of FLUXNET eddy

566 covariance observations: validation of a model tree ensemble approach using a biosphere

567 model, *Biogeosciences*, 6, 2001-2013, [doi:10.5194/bg-6-2001-2009](https://doi.org/10.5194/bg-6-2001-2009), 2009.

568 Lam, J. C., and Li, D. H. W.: Correlation between global solar radiation and its direct and diffuse

569 components, *Build Environ*, 31, 527-535, [doi:10.1016/0360-1323\(96\)00026-1](https://doi.org/10.1016/0360-1323(96)00026-1), 1996.

570 Lamarque, J. F., Shindell, D. T., Josse, B., Young, P. J., Cionni, I., Eyring, V., Bergmann, D.,

571 Cameron-Smith, P., Collins, W. J., Doherty, R., Dalsoren, S., Faluvegi, G., Folberth, G., Ghan,

572 S. J., Horowitz, L. W., Lee, Y. H., MacKenzie, I. A., Nagashima, T., Naik, V., Plummer, D.,

573 Righi, M., Rumbold, S. T., Schulz, M., Skeie, R. B., Stevenson, D. S., Strode, S., Sudo, K.,

574 Szopa, S., Voulgarakis, A., and Zeng, G.: The Atmospheric Chemistry and Climate Model

575 Intercomparison Project (ACCMIP): overview and description of models, simulations and

576 climate diagnostics, *Geosci Model Dev*, 6, 179-206, [doi:10.5194/gmd-6-179-2013](https://doi.org/10.5194/gmd-6-179-2013), 2013.

577 Le Quere, C., Andrew, R. M., Friedlingstein, P., Sitch, S., Pongratz, J., Manning, A. C., Korsbakken,

578 J. I., Peters, G. P., Canadell, J. G., Jackson, R. B., Boden, T. A., Tans, P. P., Andrews, O. D.,

579 Arora, V. K., Bakker, D. C. E., Barbero, L., Becker, M., Betts, R. A., Bopp, L., Chevallier, F.,

580 Chini, L. P., Ciais, P., Cosca, C. E., Cross, J., Currie, K., Gasser, T., Harris, I., Hauck, J., Haverd,

581 V., Houghton, R. A., Hunt, C. W., Hurtt, G., Ilyina, T., Jain, A. K., Kato, E., Kautz, M., Keeling,

582 R. F., Goldewijk, K. K., Kortzinger, A., Landschutzer, P., Lefevre, N., Lenton, A., Lienert, S.,

583 Lima, I., Lombardozi, D., Metzl, N., Millero, F., Monteiro, P. M. S., Munro, D. R., Nabel, J.

584 E. M. S., Nakaoka, S., Nojiri, Y., Padin, X. A., Peregón, A., Pfeil, B., Pierrot, D., Poulter, B.,

585 Rehder, G., Reimer, J., Rodenbeck, C., Schwinger, J., Seferian, R., Skjelvan, I., Stocker, B. D.,

586 Tian, H. Q., Tilbrook, B., Tubiello, F. N., van der Laan-Luijkx, I. T., van der Werf, G. R., van

587 Heuven, S., Viovy, N., Vuichard, N., Walker, A. P., Watson, A. J., Wiltshire, A. J., Zaehle, S.,

588 and Zhu, D.: Global Carbon Budget 2017, *Earth Syst Sci Data*, 10, 405-448, [doi:10.5194/essd-](https://doi.org/10.5194/essd-10-405-2018)

589 [10-405-2018](https://doi.org/10.5194/essd-10-405-2018), 2018.

Formatted: Indent: Left: 0 cm, Hanging: 2.02 ch, First line: -2.02 ch

Formatted: Indent: Left: 0 cm, Hanging: 2.02 ch, First line: -2.02 ch

590 Lohmann, U., and Feichter, J.: Global indirect aerosol effects: a review, *Atmospheric Chemistry and*
591 *Physics*, 5, 715-737, 2005.

592 Mann, M. E., Miller, S. K., Rahmstorf, S., Steinman, B. A., and Tingley, M.: Record temperature
593 streak bears anthropogenic fingerprint, *Geophys Res Lett*, 44, 7936-7944,
594 [doi:10.1002/2017gl074056](https://doi.org/10.1002/2017gl074056), 2017.

595 Meinshausen, M., Smith, S. J., Calvin, K., Daniel, J. S., Kainuma, M. L. T., Lamarque, J. F.,
596 Matsumoto, K., Montzka, S. A., Raper, S. C. B., Riahi, K., Thomson, A., Velders, G. J. M., and
597 van Vuuren, D. P. P.: The RCP greenhouse gas concentrations and their extensions from 1765
598 to 2300, *Climatic Change*, 109, 213-241, [doi:10.1007/S10584-011-0156-Z](https://doi.org/10.1007/S10584-011-0156-Z), 2011.

599 Mengis, N., Partanen, A.-I., Jalbert, J., and Matthews, H. D.: 1.5 °C carbon budget dependent on
600 carbon cycle uncertainty and future non-CO2 forcing, *Scientific Reports*, 8, 5831, 2018.

601 Mercado, L. M., Bellouin, N., Sitch, S., Boucher, O., Huntingford, C., Wild, M., and Cox, P. M.:
602 Impact of changes in diffuse radiation on the global land carbon sink, *Nature*, 458, 1014-U1087,
603 [doi:10.1038/Nature07949](https://doi.org/10.1038/Nature07949), 2009.

604 Millar, R. J., Fuglestedt, J. S., Friedlingstein, P., Rogelj, J., Grubb, M. J., Matthews, H. D., Skeie,
605 R. B., Forster, P. M., Frame, D. J., and Allen, A. R.: Emission budgets and pathways consistent
606 with limiting warming to 1.5 degrees C, *Nat Geosci*, 10, 741-747, [doi:10.1038/Ngeo3031](https://doi.org/10.1038/Ngeo3031),
607 2017.

608 Mitchell, D., Heavyside, C., Schaller, N., Allen, M., Ebi, K. L., Fischer, E. M., Gasparrini, A.,
609 Harrington, L., Kharin, V., Shiogama, H., Sillmann, J., Sippel, S., and Vardoulakis, S.: Extreme
610 heat-related mortality avoided under Paris Agreement goals, *Nat Clim Change*, 8, 551-553,
611 [doi:10.1038/s41558-018-0210-1](https://doi.org/10.1038/s41558-018-0210-1), 2018.

612 Mu, Q. Z., Zhao, M. S., Running, S. W., Liu, M. L., and Tian, H. Q.: Contribution of increasing
613 CO(2) and climate change to the carbon cycle in China's ecosystems, *J Geophys Res-Bioge*,
614 113, G01018, [doi:10.1029/2006jg000316](https://doi.org/10.1029/2006jg000316), 2008.

615 Nangombe, S., Zhou, T., Zhang, W., Wu, B., Hu, S., Zou, L., and Li, D.: Record-breaking climate
616 extremes in Africa under stabilized 1.5°C and 2°C global warming scenarios, *Nat Clim Change*,
617 8, 375-380, [doi:10.1038/s41558-018-0145-6](https://doi.org/10.1038/s41558-018-0145-6), 2018.

618 Piao, S. L., Fang, J. Y., Ciais, P., Peylin, P., Huang, Y., Sitch, S., and Wang, T.: The carbon balance
619 of terrestrial ecosystems in China, *Nature*, 458, 1009-U1082, [doi:10.1038/nature07944](https://doi.org/10.1038/nature07944), 2009.

620 Piao, S. L., Sitch, S., Ciais, P., Friedlingstein, P., Peylin, P., Wang, X. H., Ahlstrom, A., Anav, A.,
621 Canadell, J. G., Cong, N., Huntingford, C., Jung, M., Levis, S., Levy, P. E., Li, J. S., Lin, X.,
622 Lomas, M. R., Lu, M., Luo, Y. Q., Ma, Y. C., Myneni, R. B., Poulter, B., Sun, Z. Z., Wang, T.,
623 Viogy, N., Zaehle, S., and Zeng, N.: Evaluation of terrestrial carbon cycle models for their
624 response to climate variability and to CO2 trends, *Global Change Biol*, 19, 2117-2132,
625 [doi:10.1111/Gcb.12187](https://doi.org/10.1111/Gcb.12187), 2013.

626 Rienecker, M. M., Suarez, M. J., Gelaro, R., Todling, R., Bacmeister, J., Liu, E., Bosilovich, M. G.,
627 Schubert, S. D., Takacs, L., Kim, G. K., Bloom, S., Chen, J. Y., Collins, D., Conaty, A., Da
628 Silva, A., Gu, W., Joiner, J., Koster, R. D., Lucchesi, R., Molod, A., Owens, T., Pawson, S.,
629 Pegion, P., Redder, C. R., Reichle, R., Robertson, F. R., Ruddick, A. G., Sienkiewicz, M., and
630 Woollen, J.: MERRA: NASA's Modern-Era Retrospective Analysis for Research and
631 Applications, *J Climate*, 24, 3624-3648, [doi:10.1175/Jcli-D-11-00015.1](https://doi.org/10.1175/Jcli-D-11-00015.1), 2011.

632 Schaefer, K., Collatz, G. J., Tans, P., Denning, A. S., Baker, I., Berry, J., Prihodko, L., Suits, N., and
633 Philpott, A.: Combined Simple Biosphere/Carnegie-Ames-Stanford Approach terrestrial

634 carbon cycle model, *J. Geophys. Res.*, 113, G03034, [doi:10.1029/2007jg000603](https://doi.org/10.1029/2007jg000603), 2008.

635 Schmidt, G. A., Kelley, M., Nazarenko, L., Ruedy, R., Russell, G. L., Aleinov, I., Bauer, M., Bauer,
636 S. E., Bhat, M. K., Bleck, R., Canuto, V., Chen, Y. H., Cheng, Y., Clune, T. L., Del Genio, A.,
637 de Fainchtein, R., Faluvegi, G., Hansen, J. E., Healy, R. J., Kiang, N. Y., Koch, D., Lacis, A.
638 A., LeGrande, A. N., Lerner, J., Lo, K. K., Matthews, E. E., Menon, S., Miller, R. L., Oinas,
639 V., Oloso, A. O., Perlwitz, J. P., Puma, M. J., Putman, W. M., Rind, D., Romanou, A., Sato, M.,
640 Shindell, D. T., Sun, S., Syed, R. A., Tausnev, N., Tsigaridis, K., Unger, N., Voulgarakis, A.,
641 Yao, M. S., and Zhang, J. L.: Configuration and assessment of the GISS ModelE2 contributions
642 to the CMIP5 archive, *J Adv Model Earth Sy*, 6, 141-184, [doi:10.1002/2013ms000265](https://doi.org/10.1002/2013ms000265), 2014.

643 Sitch, S., Cox, P. M., Collins, W. J., and Huntingford, C.: Indirect radiative forcing of climate change
644 through ozone effects on the land-carbon sink, *Nature*, 448, 791-794,
645 [doi:10.1038/Nature06059](https://doi.org/10.1038/Nature06059), 2007.

646 Smith, W. K., Reed, S. C., Cleveland, C. C., Ballantyne, A. P., Anderegg, W. R. L., Wieder, W. R.,
647 Liu, Y. Y., and Running, S. W.: Large divergence of satellite and Earth system model estimates
648 of global terrestrial CO₂ fertilization, *Nat Clim Change*, 6, 306-310,
649 [doi:10.1038/Nclimate2879](https://doi.org/10.1038/Nclimate2879), 2016.

650 Solomon, S., Plattner, G.-K., Knutti, R., and Friedlingstein, P.: Irreversible climate change due to
651 carbon dioxide emissions, *P Natl Acad Sci USA*, 106, 1704-1709,
652 [doi:10.1073/pnas.0812721106](https://doi.org/10.1073/pnas.0812721106), 2009.

653 Spitters, C. J. T.: Separating the Diffuse and Direct Component of Global Radiation and Its
654 Implications for Modeling Canopy Photosynthesis .2. Calculation of Canopy Photosynthesis,
655 *Agr Forest Meteorol*, 38, 231-242, [doi:10.1016/0168-1923\(86\)90061-4](https://doi.org/10.1016/0168-1923(86)90061-4), 1986.

656 Stehfest, E., Zeist, W.-J. v., Valin, H., Havlik, P., Popp, A., Kyle, P., Tabeau, A., Mason-D'Croz, D.,
657 Hasegawa, T., Bodirsky, B. L., Calvin, K., Doelman, J. C., Fujimori, S., Humpenöder, F.,
658 Lotze-Campen, H., Meijl, H. v., and Wiebe, K.: Key determinants of global land-use
659 projections, *Nat Commun*, 10, 2166, 2019.

660 Tian, H. Q., Xu, X. F., Lu, C. Q., Liu, M. L., Ren, W., Chen, G. S., Melillo, J., and Liu, J. Y.: Net
661 exchanges of CO₂, CH₄, and N₂O between China's terrestrial ecosystems and the atmosphere
662 and their contributions to global climate warming, *Journal of Geophysical Research*, 116,
663 G02011, [doi:10.1029/2010jg001393](https://doi.org/10.1029/2010jg001393), 2011.

664 Warszawski, L., Friend, A., Ostberg, S., Frieler, K., Lucht, W., Schaphoff, S., Beerling, D., Cadule,
665 P., Ciais, P., Clark, D. B., Kahana, R., Ito, A., Keribin, R., Kleidon, A., Lomas, M., Nishina,
666 K., Pavlick, R., Rademacher, T. T., Buechner, M., Piontek, F., Schewe, J., Serdeczny, O., and
667 Schellnhuber, H. J.: A multi-model analysis of risk of ecosystem shifts under climate change,
668 *Environ Res Lett*, 8, 044018, [doi:10.1088/1748-9326/8/4/044018](https://doi.org/10.1088/1748-9326/8/4/044018), 2013.

669 Weedon, G. P., Balsamo, G., Bellouin, N., Gomes, S., Best, M. J., and Viterbo, P.: The WFDEI
670 meteorological forcing data set: WATCH Forcing Data methodology applied to ERA-Interim
671 reanalysis data, *Water Resources Research*, 50, 7505-7514, [doi:10.1002/2014wr015638](https://doi.org/10.1002/2014wr015638), 2014.

672 Wu, S., Yin, Y., Zhao, D., Huang, M., Shao, X., and Dai, E.: Impact of future climate change on
673 terrestrial ecosystems in China, *International Journal of Climatology*, 30, 866-873,
674 [doi:10.1002/joc.1938](https://doi.org/10.1002/joc.1938), 2009.

675 Xiao, J. F., Zhou, Y., and Zhang, L.: Contributions of natural and human factors to increases in
676 vegetation productivity in China, *Ecosphere*, 6, 233, [doi:10.1890/Es14-00394.1](https://doi.org/10.1890/Es14-00394.1), 2015.

677 Yao, Y. T., Wang, X. H., Li, Y., Wang, T., Shen, M. G., Du, M. Y., He, H. L., Li, Y. N., Luo, W. J.,

678 Ma, M. G., Ma, Y. M., Tang, Y. H., Wang, H. M., Zhang, X. Z., Zhang, Y. P., Zhao, L., Zhou,
679 G. S., and Piao, S. L.: Spatiotemporal pattern of gross primary productivity and its covariation
680 with climate in China over the last thirty years, *Global Change Biol*, 24, 184-196,
681 [doi:10.1111/gcb.13830](https://doi.org/10.1111/gcb.13830), 2018.

682 Yu, H., Kaufman, Y. J., Chin, M., Feingold, G., Remer, L. A., Anderson, T. L., Balkanski, Y.,
683 Bellouin, N., Boucher, O., Christopher, S., DeCola, P., Kahn, R., Koch, D., Loeb, N., Reddy,
684 M. S., Schulz, M., Takemura, T., and Zhou, M.: A review of measurement-based assessments
685 of the aerosol direct radiative effect and forcing, *Atmos. Chem. Phys.*, 6, 613-666, 2006.

686 Yue, X., and Unger, N.: The Yale Interactive terrestrial Biosphere model: description, evaluation
687 and implementation into NASA GISS ModelE2, *Geosci Model Dev*, 8, 2399-2417,
688 [doi:10.5194/gmd-8-2399-2015](https://doi.org/10.5194/gmd-8-2399-2015), 2015.

689 Yue, X., and Unger, N.: Aerosol optical depth thresholds as a tool to assess diffuse radiation
690 fertilization of the land carbon uptake in China, *Atmospheric Chemistry and Physics*, 17, 1329-
691 1342, [doi:10.5194/acp-17-1329-2017](https://doi.org/10.5194/acp-17-1329-2017), 2017.

692 Yue, X., Unger, N., Harper, K., Xia, X., Liao, H., Zhu, T., Xiao, J., Feng, Z., and Li, J.: Ozone and
693 haze pollution weakens net primary productivity in China, *Atmospheric Chemistry and Physics*,
694 17, 6073-6089, [doi:10.5194/acp-17-6073-2017](https://doi.org/10.5194/acp-17-6073-2017), 2017.

695 Yue, X., and Unger, N.: Fire air pollution reduces global terrestrial productivity, *Nat Commun*, 9,
696 5413, [doi:10.1038/s41467-018-07921-4](https://doi.org/10.1038/s41467-018-07921-4), 2018.

697 Zaehle, S., Medlyn, B. E., De Kauwe, M. G., Walker, A. P., Dietze, M. C., Hickler, T., Luo, Y. Q.,
698 Wang, Y. P., El-Masri, B., Thornton, P., Jain, A., Wang, S. S., Warlind, D., Weng, E. S., Parton,
699 W., Iversen, C. M., Gallet-Budynek, A., McCarthy, H., Finzi, A. C., Hanson, P. J., Prentice, I.
700 C., Oren, R., and Norby, R. J.: Evaluation of 11 terrestrial carbon-nitrogen cycle models against
701 observations from two temperate Free-Air CO₂ Enrichment studies, *New Phytol*, 202, 803-
702 822, [doi:10.1111/Nph.12697](https://doi.org/10.1111/Nph.12697), 2014.

704 **Author Contributions**

705 X.Y., H.L., and H.W. designed the research and wrote the manuscript. X.Y. downloaded CMIP5
706 data, set up models, and performed all simulations. T.Z. evaluated diffuse radiation models.
707 N.U. provided ACCMIP data. S.S. provided TRENDY data. Z.F. provided O₃ damaging meta-
708 analysis data in China. J.Y. analyzed TRENDY results over China. All authors contributed to
709 the interpretation of the results and improvement of the paper.

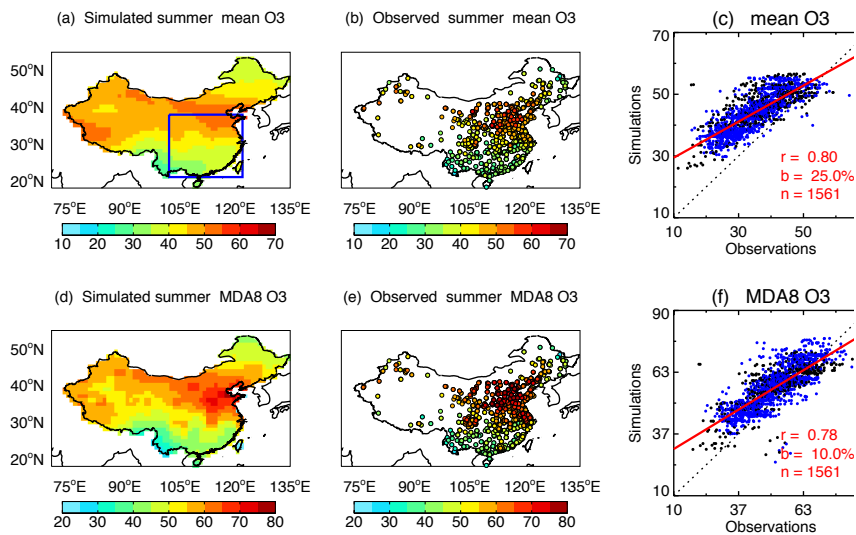
711 **Acknowledgements**

712 This work is supported by the National Key Research and Development Program of China (grant
713 no. 2017YFA0603802) and National Natural Science Foundation of China (grant no. 91744311,
714 [41975155](https://doi.org/10.1111/gcb.13830)).

Deleted: .

Formatted: Indent: Left: 0 cm, Hanging: 2.02 ch, First line: -2.02 ch

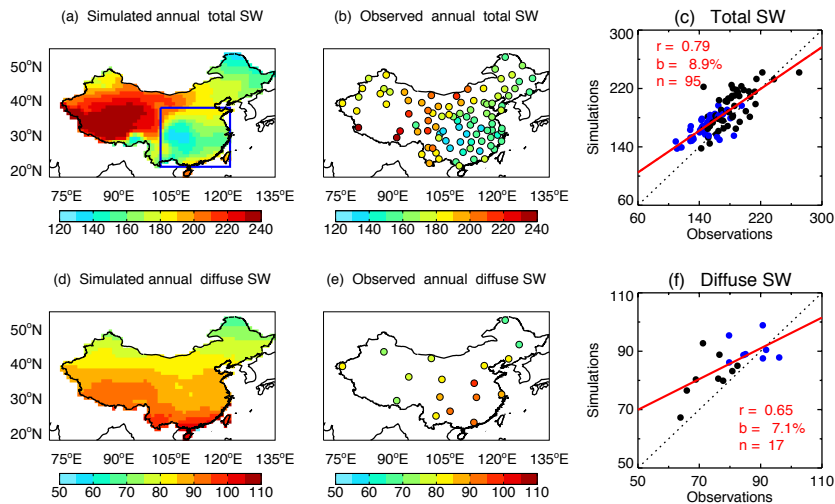
Deleted: .



719
 720 **Figure 1.** Evaluation of surface O₃ with site-level observations. Simulations are ensemble (a) mean
 721 and (d) daily maximum 8-hour average (MDA8) O₃ for the period of 2005-2015 from 12 ACCMIP
 722 models. Observations (b and e) are the average during 2015-2018 from 1580 sites operated by
 723 Ministry of Ecology and Environment, China. The correlation coefficients (r), relative biases (b),
 724 and number of sites (n, excluding data-missing sites) are shown in the scatter plots (c and f). The
 725 blue points in the scatter plots represent sites located within the box regions in eastern China as
 726 shown in (a). The dashed line represents the 1:1 ratio. The red line is the linear regression between
 727 simulations and observations.

728

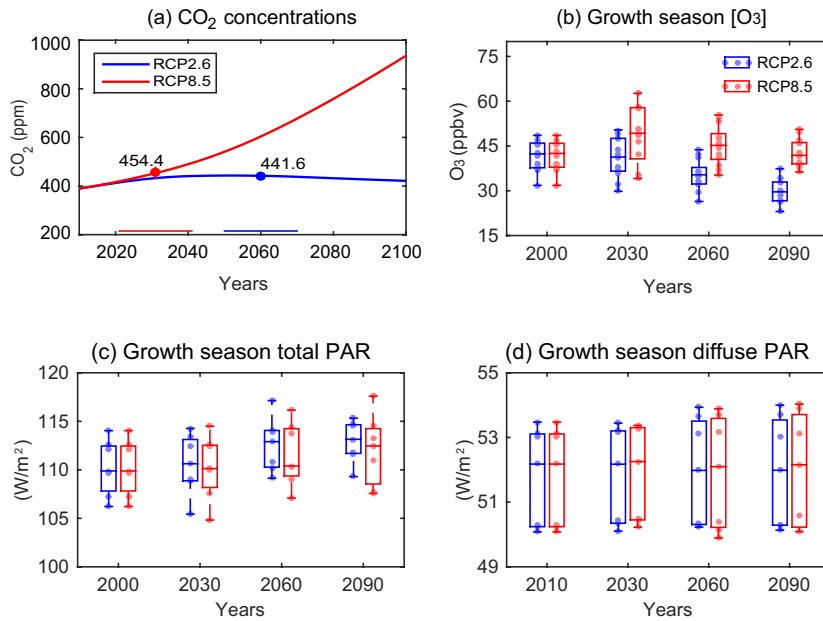
729



730
 731 **Figure 2.** Evaluation of radiation fluxes with site-level observations. Simulations are surface (a)
 732 total shortwave radiation (W m^{-2}) and (d) diffuse radiation derived with method M01 (Table S4) for
 733 the period of 2005-2015 from an ensemble of 7 CMIP5 climate models. Observations (b and e) are
 734 the average during 2009-2011 from 106 sites operated by the Climate Data Center, Chinese
 735 Meteorological Administration. The correlation coefficients (r), relative biases (b), and number of
 736 sites (n , excluding data-missing sites) are shown in the scatter plots (c and f). The blue points in the
 737 scatter plots represent sites located within the box regions in eastern China as shown in (a). The
 738 dashed line represents the 1:1 ratio. The red line is the linear regression between simulations and
 739 observations.

740
 741

742
743

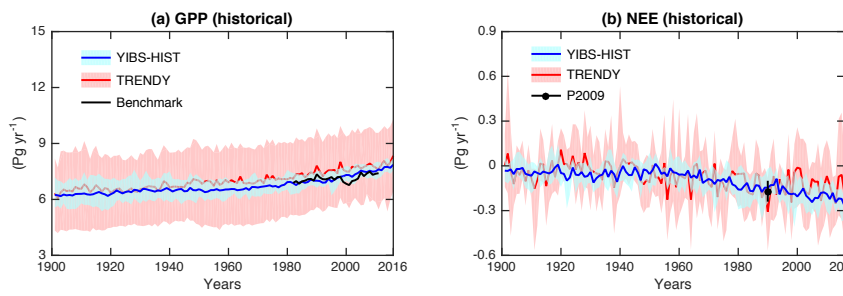


744
745
746
747
748
749
750
751
752
753
754
755
756
757
758
759
760
761

Figure 3. Changes in atmospheric compositions and radiation. Results shown are projected future (a) global CO₂ concentrations, and (b) surface O₃ concentrations, (c) total Photosynthetically Active Radiation (PAR), and (d) diffuse PAR at growth season in China. The average (a) CO₂ concentrations at the global warming of 1.5°C are 442 ppm for RCP2.6 scenario (blue, 2050-2070) and 454 ppm for RCP8.5 scenario (red, 2021-2041). The (b) O₃ concentrations are averaged over east of 110°E in China from 12 ACCMIP models for RCP2.6 (blue) and RCP8.5 (red) scenarios. Each dot represents the value averaged for May to September from a chemistry model. The (c-d) PAR values are averaged over China from 7 CMIP5 models for RCP2.6 (blue) and RCP8.5 (red) scenarios. Diffuse PAR is calculated using hourly total PAR and solar zenith angle based on the parameterization M01. Each dot represents the value averaged for May to September from a climate model. For each selected year in (b-d), a period of 11 years (5 years before and 5 years after) is used to derive the decadal mean values.

762

763



764

765 **Figure 4.** Historical carbon fluxes in China. Results shown are simulated (a) gross
766 primary productivity (GPP) and (b) net ecosystem exchange (NEE) during historical
767 period (1901-2016) using YIBs model (blue), and the comparison with predictions of
768 14 terrestrial models from TRENDY project (red). The bold lines are ensemble means
769 with red shadings for inter-vegetation-model uncertainties and blue shadings for inter-
770 climate-model uncertainties. All YIBs simulations are driven with daily meteorology
771 from CMIP5 models. All TRENDY simulations are driven with CRUNCEP
772 meteorology. The black line in (a) represents benchmark results of 1980-2011 from
773 Jung et al. (2009). The black point with error bar in (b) represents the synthesis of
774 ground- and model-based estimate of NEE in China by Piao et al. (2009).

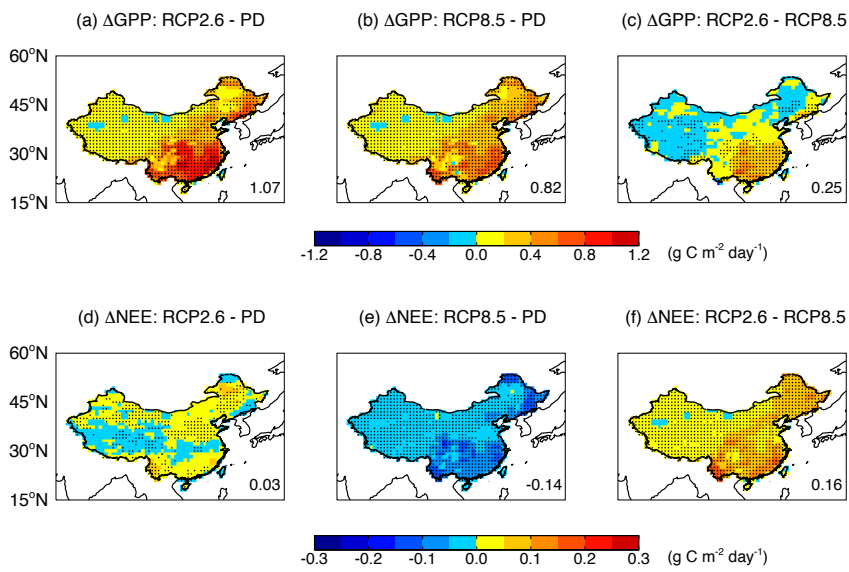
775

776

777

778

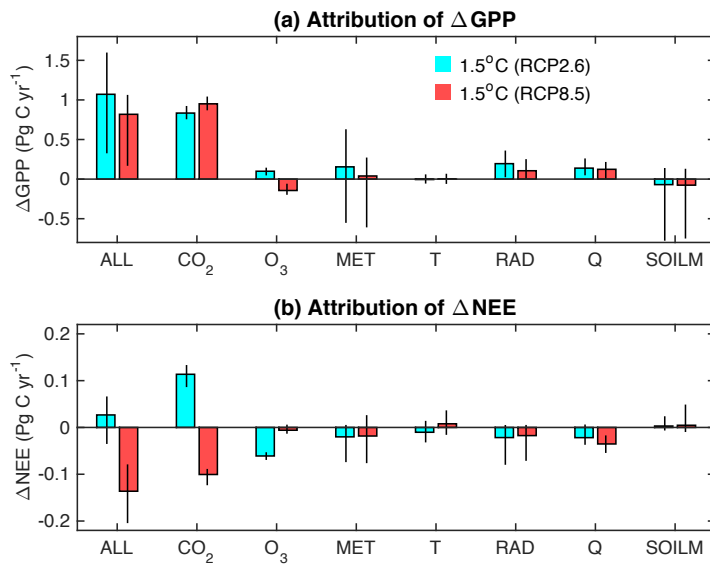
779



780

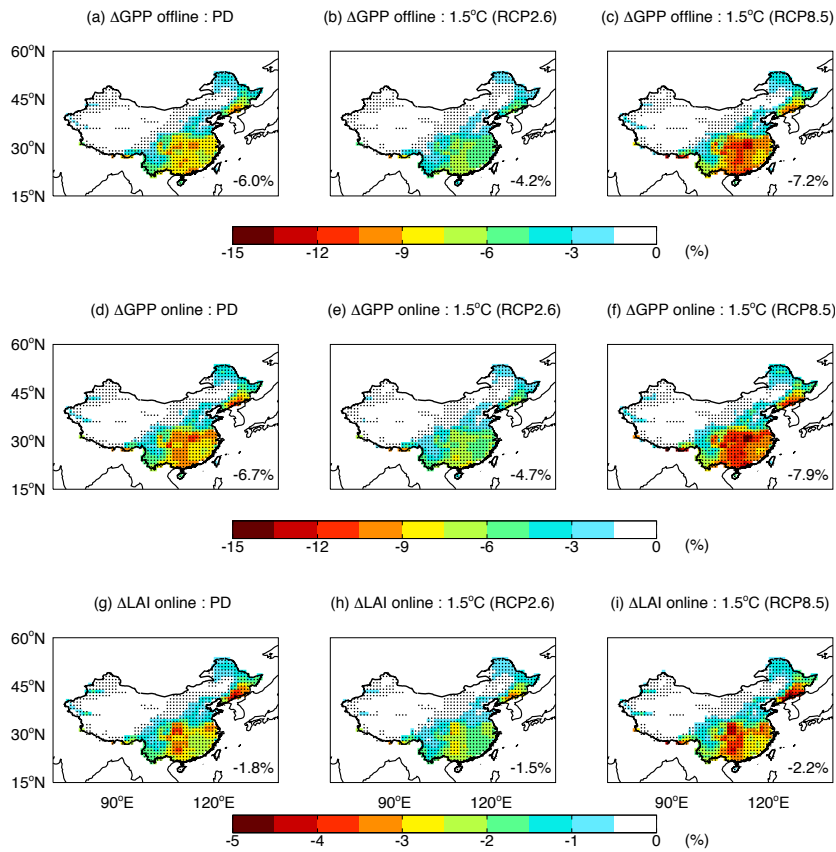
781 **Figure 5.** Changes in carbon fluxes by global warming of 1.5°C. Results shown are
782 simulated (top) GPP and (bottom) NEE over China between the period of global
783 warming of 1.5°C and present day (1995-2015) under (left) RCP2.6 scenario, (middle)
784 RCP8.5 scenario, and (right) their differences. The period of global warming of 1.5 °C
785 is set to 2050-2070 for RCP2.6 and 2021-2041 for RCP8.5. Simulations are performed
786 using YIBs vegetation model driven with daily meteorology from 7 CMIP5 models.
787 The O_3 damaging effect is included with predicted ensemble O_3 concentrations from 12
788 ACCMIP models. For each grid, significant changes at $p < 0.05$ are marked with dots.
789 The total changes (Pg C yr^{-1}) over China are shown in each panel.

790

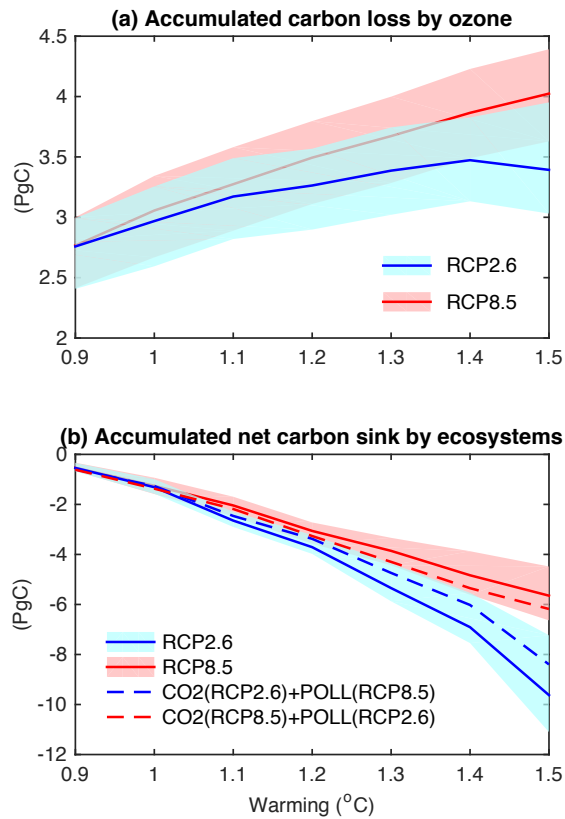


791
 792 **Figure 6.** Attribution of changes in GPP and NEE to individual driving factors. Results
 793 shown are the predicted GPP changes in China between the period of global warming
 794 of 1.5°C and present day (1995-2015) caused by all (ALL) or individual driving factors,
 795 including CO₂ fertilization, O₃ damaging, and meteorological changes (MET). The
 796 perturbations by meteorology is a combination of those by temperature (T), radiation
 797 (RAD), specific humidity (Q), and soil moisture (SOILM). The contrast is shown
 798 between the scenarios of RCP2.6 (blue, 2050-2070) and RCP8.5 (red, 2021-2041). The
 799 error bars indicate uncertainties of YIBs simulations using different future meteorology
 800 from 7 CMIP5 models.

801
 802
 803



804
 805 **Figure 7.** Damaging effects of O₃ to photosynthesis and plant growth. Results shown are ensemble
 806 mean changes in (top) offline GPP, (middle) online GPP, and (bottom) leaf area index (LAI) caused
 807 by O₃ at (left) present day (1995-2015) and 1.5°C warming under (middle) RCP.6 (2050-2070) and
 808 (right) RCP8.5 (2021-2041) scenarios. The simulations are performed with YIBs vegetation model
 809 driven with meteorology from 7 CMIP5 models and hourly ozone derived from 12 ACCMIP models.
 810 The damaging effect is averaged for high and low O₃ sensitivities. For each grid, significant changes
 811 at $p < 0.05$ are marked with dots. The mean changes over China are shown in each panel.
 812



814
 815 **Figure 8.** Accumulated carbon budget in China by 1.5°C global warming. The top panel
 816 shows the total carbon loss of ecosystems caused by O₃ damaging effects at different
 817 warming thresholds for two emission pathways. The bottom panel shows the
 818 accumulated net carbon sink by ecosystems in China at the 1.5°C global warming. The
 819 two solid lines represent emissions of CO₂ and pollutants from the same scenario, either
 820 RCP2.6 (blue) or RCP8.5 (red). The dashed lines represent sensitivity experiments with
 821 inconsistent CO₂ and pollutants, with the blue (red) line driven with CO₂ from RCP2.6
 822 (RCP8.5) but air pollution from RCP8.5 (RCP2.6). The warming of 1.0 °C is the year
 823 2010 for both RCP2.6 and RCP8.5 scenarios.

824

825